Bioprinting 45 (2025) e00377

Contents lists available at ScienceDirect

Bioprinting

journal homepage: www.sciencedirect.com/journal/bioprinting

Zirconia-calcium silicate bioactive composites for dental applications using DLP additive manufacturing

Ahmed Binobaid [a,b], Michele De Lisi [b], Josette Camilleri [c], Hany Hassanin [d,*], Khamis Essa [b,**]

[a] School of Dentistry, King Saud Bin Abdulaziz University for Health Sciences, Riyadh, Saudi Arabia
[b] School of Mechanical Engineering, University of Birmingham, Birmingham, B15 2TT, UK
[c] School of Dentistry, University of Birmingham, Birmingham, B15 2TT, UK
[d] School of Engineering, Technology, and Design, Canterbury Christ Church University, Canterbury, CT1 1QU, UK

ARTICLE INFO

Keywords:
Zirconia-calcium silicate composites
Digital light processing
Bioactive materials
Additive manufacturing
Printing optimization

ABSTRACT

Zirconia has outstanding mechanical strength which made it a favourable material dental implants material. However, its use is limited by challenges in bone bonding and elasticity. This paper introduces a novel bioprinting ceramic material by mixing calcium silicate with zirconia to enhance bioactivity. Using the high precision and speed of Digital Light Processing (DLP), this study develops a novel zirconia-calcium silicate slurry for dental applications. The study reports the preparation of zirconia-calcium silicate, formulation of resin compositions, and optimization of the bioprinting, debinding and sintering. Employing a full factorial Design of Experiments (DOE), a systematic approach was implemented to identify optimal printing conditions such as the layer thickness, exposure time, and power. The results show that slurries formulated with BYK-111 as the dispersant and ACMO/PEGDA/TPO resin, coupled with 80 wt% solid loading, achieved the most favourable rheological properties, cure depth, and printing accuracy. The optimal printing conditions were 0.75 s exposure time, 300 % exposure power, and 30 μm layer thickness, ensured a relative density of the sintered implants exceeding 95 %. This study advances dental implant materials by introducing a novel DLP biomaterial with a slurry formulation, presenting significant implications for clinical applications and future research in developing advanced dental and medical implants.

1. Introduction

Dental implant materials have seen advancements in recent years, especially with the emerging additive manufacturing technologies. Losing one or more teeth can affect not only a person's appearance and ability to eat but also their confidence and wellbeing [1]. The ability to communicate clearly can be significantly affected by the loss of anterior teeth. Furthermore, the loss of a tooth leaves a space between the teeth that eventually causes dental malocclusion owing to neighbouring teeth beginning to drift away, necessitating orthodontic intervention [1,2]. In dentistry, there are approaches to treating missing teeth. Depending on the patient conditions, the dentist may choose to treat the patient with a complete denture or a removable/fixed prosthesis. Every dental treatment has benefits and drawbacks of its own. One of the main disadvantages of dental implants is that they are considered expensive in comparison to other dental treatments options [3]. In dentistry, ceramics and metals are the main two materials used widely to restore missing teeth. Dental crowns, bridges, and implants are made of either ceramics or metals and can be used to restore teeth functionally or aesthetically [4]. Lately, the use of Porcelain Fused to Metal (PFM) restorations has become a key approach, especially for crowns and bridges. On the other hand, zirconia, with its biocompatibility, natural appearance, and superior mechanical properties, has become a widely used dental biomaterial in recent years [5]. Since the introduction of Additive Manufacturing several years ago, Digital Light Processing has developed into a fully advanced and sophisticated production technology with computer-aided design/manufacturing (CAD/CAM). Importantly, it has the ability to fabricate ceramic objects with extreme printing precision, which makes it a competitive method with promising potential to be used in dentistry [6].

Additive manufacturing has the potential to complement or even replace some conventional manufacturing methods. It allows dental

* Corresponding author.
** Corresponding author.
E-mail addresses: hany.hassanin@canterbury.ac.uk (H. Hassanin), k.e.a.essa@bham.ac.uk (K. Essa).

https://doi.org/10.1016/j.bprint.2024.e00377
Received 26 September 2024; Received in revised form 24 November 2024; Accepted 29 November 2024
Available online 7 December 2024

professionals to fabricate accurate structure, rapidly and at a lower cost [7]. The process involves slicing a CAD model into thin layers and then sequentially adding those layers to create a three-dimensional object [8]. First, Standard Tessellation Language (STL) files are used to encode the CAD data, with the slicing software then transforming the data into a succession of 3D layers. Afterward, at the printing stage, the selected biomaterial is added layer by layer by the Additive Manufacturing machine until the desired physical item is created. Additive manufacturing can achieve high resolutions, which makes it suitable in the fabrication of extremely complicated biostructures, such as dental implants. Recently, the Additive Manufacturing of ceramics has been seen to increase, with a promising potential market introduced. The AM method offers limitless possibilities for manufacturing, complete with a wide range of materials, and is currently viewed as a vital tool for biotechnology innovation [9,10]. Indirect and direct are the two main categories of ceramic AM approaches: the indirect approach includes methods like Stereolithography (SLA) and Direct Inkjet Printing (DIP), where a binder or photopolymer is used, and the final ceramic object is obtained after a debinding and sintering process. Direct approaches, on the other hand, include techniques like Selective Laser Sintering (SLS) and Laminated Object Manufacturing (LOM), where ceramic materials are directly shaped into the final object without the need for a binder [5–7]. One of the main advantages of AM is to achieve high complex shaped geometries which could potentially assist for a better outcome in many fields [11]. Digital Light Processing (DLP) of ceramics involves precise control over the slurry composition to achieve high-resolution and accurate 3D printed parts, followed by debinding and sintering. The slurries used on DLP of zirconia consist of the ceramic filler, photoinitiator, and binder. The interactions between the slurry materials can affect the properties of the printed components. For example, if there is a large index of refraction mismatch between the resins and the ceramic particles, it can lead to issues with cure depth and can ultimately impact the precision and accuracy of the final part [12,13].

The selection and the ratio of slurry composition affect the curing behaviours, which in turn affects the properties of the printed object. Several studies introduce the process of ceramic slurries preparation enabling them for DLP additive manufacturing. The surface of the used ceramic particles can be pre-treated [14,15] or used directly without pre-treatment [16–18], prior to adding resin. Typically, high solid loading of ceramic slurries can increase the density, improve geometrical accuracy of the printed object, and reduce the shrinkage after sintering However, achieving this goal is a challenge as increasing the solid loading could significantly increase viscosity and affect the printability. Nonetheless, this issue could be mitigated by optimising the dispersant, as it would create steric or electrostatic barriers between particles and prevent agglomeration, whilst at the same time homogenising the ceramic filler dispersion [19,20]. Dental implants and prostheses require high aesthetic quality and precision to ensure a natural appearance and proper fit, though their longevity and success depend more on material durability and proper integration with the bone. This would make DLP a strong candidate as one of the high accuracy and resolution additive manufacturing. Various materials can be used in DLP slurries, including photopolymer resins, zirconia, and calcium phosphate. In addition, other printable materials that have been utilised include titanium metals, glass-filled resins, and nano-composite resins. During the DLP process, dimensional accuracy is determined by intricate relationships amongst printer resolution, process parameters, and photopolymerisable slurry composition [21,22].

Recently, there has been research conducted on the application of zirconia as a biocompatible material using techniques such as DLP, SLA, SLS and SLM [23]. High precision and smooth surface finishes, which are crucial for dental restorations, have been successfully achieved. Furthermore, it successfully achieved complex designs and implemented appropriate customisation to improve the manufacturing process of implants and prostheses that could be tailored to individual patients [24]. Zirconia is a high-performance ceramic known for its strength, wear resistance, and precision, making it ideal for electronics and healthcare. However, its brittleness and limited bioactivity pose challenges in biomedical applications [25–27]. Calcium silicate (Ca_2SiO_4) has an excellent bioactivity, osseointegration, and promotes bone regeneration, making it very appropriate for applications in bone scaffolds and dental applications [28]. Additionally, it possesses the capability to generate scaffolds with appropriate porosity and mechanical characteristics that are comparable to those of natural bone. Hanxu Zhang et al. showed that adding calcium silicate could prove beneficial to enhancing the printed prosthesis's biocompatibility whilst tailoring its properties and characteristics to the desired values [29]. Sheng Yang & Ping Wu reported that calcium silicate can improve both mechanical, as well as the biological, properties [30]. DLP, SLA and 3D Bioprinting have successfully printed calcium silicate components and fabricated scaffolds that include living cells within calcium silicate matrices for tissue engineering purposes. Calcium silicate generally exhibits weaker mechanical strength in comparison to zirconia, which restricts its employment in load-bearing applications. Additionally, achieving degradation rates that align with tissue regeneration rates is a significant difficulty. Much like zirconia, calcium silicate also experiences shrinkage problems during debinding and sintering [31]. Incorporating calcium silicate as a composite for zirconia can significantly enhance these properties, improving the material's durability and promoting better biological integration. According to Ding et al. (2021), zirconia calcium silicate has the ability to enhance bioactivity without causing a major reduction in its mechanical qualities [32]. However, the achievement of these characterises relies heavily on the homogeneity of the mixture and the thermal post-processing techniques.

While literature shows that the use of calcium silicate with zirconia shows great promise in enhancing bioactivity and overall performance, there is a lack of studies focused on developing zirconia-calcium silicate slurries tailored for DLP. Current research primarily investigates zirconia-calcium silicate composites using traditional powder processing methods, overlooking the potential benefits of these materials within the context of additive manufacturing techniques like DLP. This leaves a critical research gap of how these materials behaves in a DLP context and how to formulate it. This paper introduces the development and optimization of a DLP zirconia calcium silicate composite slurry for dental applications. A full DoE was used to explore the influence of layer thickness, exposure power, and exposure time on the printed samples. The sample structure, mechanical characteristics, and printing accuracy were all examined. It will also establish optimal printing parameters and the debinding process to achieve 3D printed zirconia calcium silicate composite suitable for use as dental implant.

2. Materials and methods

2.1. Ceramic powder pre-treatment

In the present study, the slurry was prepared by using zirconia powder (D50 ~200 nm) (Dongguan SAT nano Technology, Guangdong, China), which was mechanically pre-treated in a ball milling machine (HMK-1901, Dandong HMKTest Instrument Co., LTD., Dandong, Liaoning, China). The X-ray Diffraction (XRD) test was carried out using the PANalytical Empyrean Diffractometer (Malvern Panalytical, Almelo, Netherlands) using Cu Kα radiation and the intensity of scattered X-rays was recorded in a 2θ-range of 20°–80°.The results presented in Fig. 1 a revealed that yttria-stabilized zirconia (YSZ) particles of (D50 ~200 nm) size had unique peak shapes typical of a tetragonal phase. This proved that YSZ had crystal structure and was stable in this phase. The Scanning Electron Microscopy (SEM) image in Fig. 1 b indicated a consistent morphology, with well-dispersed particles indicating effective synthesis. These results confirm the structural stability and uniformity of YSZ, which makes it appropriate for advanced applications. The compressive strength was evaluated by using universal testing Machine (Model no. 3369 Instron, Canton, MA, USA).

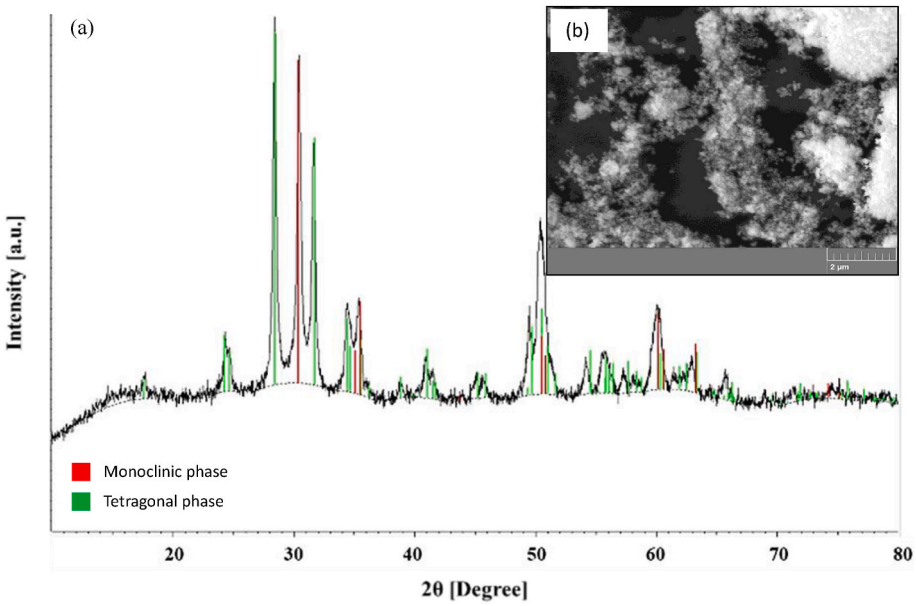

Fig. 1. (a) XRD patterns of nanozirconia powder (b) SEM image illustrating particles size distribution and particle morphology.

The process starts from nano-sized zirconia particle, ball mill them and sift them by a 250-μm sieve. The as-received powder was ball milled with 7 mm zirconium oxide as grinding media (Fullbrook Systems, Hemel Hempstead, UK). The ball-to-powder (BPR) ratio was 1:1, whilst the rotating speed was set at 600 rpm for 2 h. Subsequently, the obtained powder was sifted with 250-μm mesh screen. Nano-calcium silicate powder (Nanoshel (UK) Limited, Cheshire, England) was added at a later stage in three different proportions. The addition of the Ca_2SiO_4 powder (D50 ~80 nm) was in mind of exploring the best possible mechanical properties of the mixed composite.

2.2. Preparing slurries

A ready-made ADMATEC resin (Admatec Europe BV, Alkmaar, The Netherlands) was utilised in the first slurry preparation investigation group. The second resin was formulated in-house, by mixing 4-acryloylmorpholine (ACMO) and polyethylene glycol diacrylate (PEGDA). Different dispersants were also explored in this study for obtaining the optimal slurry's rheological performance. Diphenyl (2,4,6-trimethylbenzoyl) phosphine oxide (Sigma Aldrich, Gillingham, UK) was added to the resin mixture in the amount of 1.0 wt% of the photoreactive resin. The effects of the composition combinations were studied to examine the impact of the slurry composition in relation to the material printability. Two different dispersants, BYK-111 and BYK 145 (BYK Chemie, Wesel, Germany) were used in the slurry optimization procedure, with two different base resins also examined. Importantly, the literature widely emphasises that the green body density, as well as the suspension's curing ability, can both be improved by including appropriate and homogeneous dispersion of ceramic powders in the suspension [30–32]. Accordingly, different ceramic loadings at different weight percentages—specifically 70 wt%, 75 wt%, and 80 wt% were also evaluated.

The monomers were mixed using an overhead mixer at room temperature. After the required mixture was made, the dispersant was added and mixed further. To ensure homogeneity and thorough blending, the zirconia powder was incrementally incorporated until a 75 wt% of solid loading was achieved, followed with photoinitiator and further mixing using a mechanical mixer until the mixture became homogeneous. The zirconia media was then added to the obtained slurry with a 1:1 ratio to further improve homogenisation. The mixture along with the media was then placed in a Turbula® mixer for 24 h. After the determining the best zirconia-based slurry composition at a later stage of the experimental campaign, the calcium silicate was then added in three different ratios, particularly 10 wt%, 30 wt%, and 50 wt% to be tested further. Before the actual printing of the obtained slurries, the mixture was processed for 10-min with vacuum degasser. Firstly, the study started the investigation by using only pure zirconia, different types of base monomers/resins, dispersants, and solid loadings. After selecting the best composition for the required purpose, the calcium silicate was then added. The investigated parameters and compositions are listed in Table 1 below. For precautionary measurement, the containers were kept sealed throughout the mixing process [33].

The two dispersants were mixed with the in-house produced resin, and two slurries were made, respectively. The same two dispersants were also examined with the second commercial resin, with two more slurries then prepared. The solid loading in all four cases was 75 wt%. These trials were conducted to test the influence of using different dispersants and resins on the obtained slurries and accordingly select the composition with the best printing accuracy, rheological behaviour, and cure depth properties. After determining the best composition at 75 wt% solid loading, three different zirconia solid loadings were tested to explore the solid content workability range. To test the rheological behaviour, an AR 500 machine (TA Instruments, New Castle, DE, USA) with a 20 mm parallel plate geometry was used. According to the expected printing conditions, the rheology test was conducted at a constant temperature of 20.0 °C whilst the shear rate ranged from 0.1 to 300 s^{-1} when analysing the rheological properties of slurries.

2.3. DLP printing

Samples printing was carried out by using Admaflex 130 (Admatec Europe BV, Alkmaar, The Netherlands). This 3D printer can achieve a high resolution by using a source of light that operates at a wavelength of $\lambda = 405$ nm. It is a Digital Light Processing device consisting of thousands of mirrors. The machine possesses a foil system to transfer the slurry/suspension from the slurry reservoir to the curing area in the middle of the foil run and finally to the scraper zone. The slurry is then once again pumped back to the reservoir and into the platform to cure the following layer until the full desired objective is achieved. The cure depth at different exposure powers was measured to determine the appropriate exposure power in relation to the cure depth. Whilst layer thickness is the height of the cured layer in micrometre and exposure

Table 1
The slurry preparation composition.

Base Resin	ACMO+PEGDA	ADMATEC	
Dispersant	BYK-111	BYK-145	
ZrO_2 Solid loading	70 wt.%	75 wt.%	80 wt.%
Ca_2SiO_4 Solid loading	10 wt.%	30 wt.%	50 wt.%

time indicates how long a single layer of the cured slurry is cured by the light source, the exposure power pertains to the density of the surface energy applied to the slurry per second. Utilising Jacob's equation, the cure depth (C_d) can be seen to be related to the energy dose (E):

$$C_d = D_p \ln (E/E_c)$$

where D_p is the penetration depth [34], E_c represents the critical energy required to initiate polymerisation, and E is the surface exposure energy density [35]. According to published literature, E_c and D_p represent resin-specific metrics that are independent of the exposure parameters [36]. To evaluate the exposure time and power effect on the obtained composites, a checkboard shape layer of the prepared slurries is cured. The 75 wt% slurry was employed for all initial trials. The exposure time and exposure powers that were examined to understand the curing behaviour are shown in Table 2.

After curing the checkboard layer according to the curing parameter shown in the table above, the cured layer thickness was measured by using a portable micrometre (Mitutoyo Digimatic Micrometre, MDC-25PX, Kawasaki, Japan). The average cure depth and standard deviation were found after collecting five consecutive measurements. Since the outcome from the samples' exposure time above 1 s did not provide suitable curing accuracy, the exposure time was reduced in the following stage. Table 3 shows the exposure times and powers selected to investigate the effect of the solid loadings for both of the70 wt% and 80 wt% solid loadings.

After determining the optimal solid loading content, three different ratios of nano-dicalcium silicate were added to the selected solid loading mixture for further slurry investigation. The chosen experimental variables were layer thickness, exposure time, and exposure power. To create an experimental plan, a full factorial Design of Experiments (DoE) was created to confirm how printing parameters affected the dimensional accuracy. According to the obtained cure depth results, testing parameters were adjusted to improve the DLP printing outcome. This is due to either insufficient slice curing or over-curing. The exposure power levels were modified to be 200 ‰, 300 ‰, and 400 ‰, whilst exposure time ones were modified to 500 ms, 750 ms, and 1000 ms to achieve the optimum cure depth. Three different values of each factor were then selected. The Full factorial Design of Experiments is shown in detail in Table 4.

In total, five discs were attempted to be printed for each set of conditions. The samples were designed in CAD with a thickness of 1.5 mm and a diameter of 7 mm. The files were then converted to STL file and sliced to the corresponding layer thickness. The slurry was poured into the reservoir and allowed to spread across the foil of the printing machine. From the machine settings option, the layers were permitted to settle for enough time before exposure by setting the delay after exposure to 3000 ms. On the machine sitting options, the building platform was raised and lowered every time by 7 mm at a speed of 2.5 mm/s. Finally, printed samples were taken off the building platform and cleaned with isopropanol.

Table 2
Curing parameters investigated with 75 wt% solid loading.

Exposure power [‰]	200	400	600
Exposure time [s]	1	2	3

Table 3
Curing parameters investigated for the 70 wt% and the 80 wt% solid loadings.

Exposure power [‰]	200	400	600
Exposure time [ms]	250	500	1000

Table 4
The full factorial Design of Experiments (DoE) planned for the DLP experiment.

Factors			
Exposure time [ms]	500	750	1000
Layer thickness [µm]	20	25	30
Exposure power [‰]	200	300	400
Experiment	**[‰]**	**[ms]**	**[µm]**
1	200	500	20
2	200	500	25
3	200	500	30
4	200	750	20
5	200	750	25
6	200	750	30
7	200	1000	20
8	200	1000	25
9	200	1000	30
10	300	500	20
11	300	500	25
12	300	500	30
13	300	750	20
14	300	750	25
15	300	750	30
16	300	1000	20
17	300	1000	25
18	300	1000	30
19	400	500	20
20	400	500	25
21	400	500	30
22	400	750	20
23	400	750	25
24	400	750	30
25	400	1000	20
26	400	1000	25
27	400	1000	30

2.4. Thermal post-processing

In post-processing 3D printed parts, removing the mixed resin and additives from the obtained cured sample particles is essential to obtain the required mechanical strength. The Thermogravimetric Analysis (TGA) and Differential Scanning Calorimetry (DSC) tests were conducted to track the mass loss of the green body, as well as the critical temperatures for the binder removal. At certain temperatures revealed by this test, the organic parts of the green body decompose accordingly. To identify the required temperature and establish the debinding progress, the test was conducted at a heating rate of 5 °C/min. Following the TGA results analysis, the debinding regimes were decided in line with the TGA/DSC endothermic peaks to determine the ideal process conditions. In mind of increasing the samples' strength, a pre-sintering process at 900 °C was also adopted. The debinding cycles were then carried out in a tube furnace (TSH/15/75/450, Elite Thermal Systems Ltd., Market Harborough, United Kingdom).

The debinded brown samples presenting optimal properties were

finally tested at two different sintering temperatures: the first group was sintered in an air sintering furnace (HTF 17/27, Carbolite Gero, Sheffield, UK) at 1500 °C; the second group was sintered at 1300 °C in the same furnace. Fig. 2 provides an illustrative overview of all the processes involved in the experiment.

3. Results and discussion

3.1. Curing behaviour

At various exposure times and powers, the slurries' cure depth was investigated for all tested groups with different resins and dispersants. The obtained results are shown in Fig. 3 below. The samples were cured in a checkboard pattern for a layer and the cure depth was measured. The result shows that the cure depth generally increases with an increase in led power, with the slurries containing ADMATEC resin showing a slightly higher cure depth. However, it was evident that the printing accuracy of the slurries containing ADMATEC resin was poor compared to the ACMO/PEGDA ones. During the checkboard layer curing, it was noted that the samples cured with the high exposure time and power had over cured, as can be seen in Fig. 4 below. Despite the used resin, the slurries containing BYK-145 dispersant showed lower accuracy and printing capabilities in comparison to the BYK-111 group. In the case of BYK-145 dispersant, most of the samples printing resolution would not be appropriate for the required purposes, i.e. dental prosthesis and restorations, which require extremely high precision so as to avoid any expected complications [34]. The high accuracy of the 3D printing of medical applications is not only crucial, but also extremely important in mind of expanding the prosthesis lifespan and assisting in preventing the printed unit failure [37]. Taking such facts into consideration, all four groups progressed in the experimental campaign to undertake rheological testing.

3.2. Rheology behaviour

The rheology testing was made on all four prepared slurry groups. At this stage, the solid loading was fixed to 75 wt%, with all tested slurries seen to act in a relatively similar way. The rheology test showed that the slurries experienced a decrease in viscosity with an increase in the shear rate, hence exhibiting a shear-thinning behaviour. The viscosity was not seen to be significantly affected when shear rate is higher than 20 s^{-1}. This phenomenon would assist in the printing process and is recommended by both Admaflex 130 manufacturers, as well as literature [38]. From the obtained rheology graph (Fig. 5), it can be seen that the slurry composition prepared from ACMO/PEGDA resin and BYK-111 dispersant are a suitable candidate. Given the doctor blade gap used during printing, this slurry formulation provides optimal flow characteristics, ensuring smooth and consistent printing. Based on the obtained results, the slurry composition with 75 % zirconia, BYK-111 dispersant, and ACMO/PEGDA/TPO resin was chosen for further study. Using this composition, the slurry demonstrated better properties compared to the other formulations in terms of flow characteristics. The rheological properties indicated that it maintains the desired consistency and flow behaviour, making it the most suitable candidate for achieving high-quality and precise prints in the study.

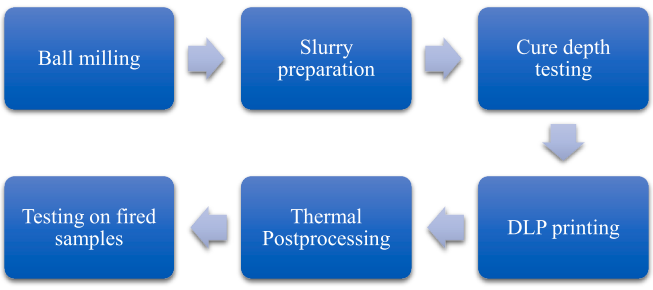

Fig. 2. The slurry preparation procedure.

3.3. Solid loading

The solid loading was also varied to identify the optimal value that balances viscosity and print quality. To characterise this, slurries with 80 wt% and 70 wt% solid loading were prepared, using the same dispersant and resin composition as in the selected formulation. This approach allowed for an evaluation of how different solid loading levels affect cure depth and overall performance, helping to identify the ideal formulation for high-quality printing. The exposure time levels were modified to 500 ms, 750 ms and 1000 ms. For each tested group, the slurries' cure depth was measured and analysed, as presented in Fig. 6 a. Conversely, it was observed that slurries cured with exposure power exceeding 400 % exhibited significantly reduced dimensional accuracy in printing. This could be mainly related to the scattering behaviour of the zirconia powder, which leads to light reflection and ununiformed distribution of the light and therefore inaccurate curing of the layers [34]. However, the samples cured with exposure power equal to and below 400 % would exhibit better printing accuracy, as presented in Fig. 6 a. It is crucial for successful dental treatment to have high accuracy of the fabricated unit. In fact, a small gap or extremely small open margin between the artificial unit and the prepared tooth could ultimately lead to complete failure in terms of long-term patient treatment [39]. In dentistry, the dental artificial unit utilised should fit perfectly if it is to function properly. Inadequate marginal integrity can result in complications such as periodontal disease, soft tissue irritation, inflammation, and gingival recession [40,41].

Following the selection of the ideal composition and adjusting the weight percentage content, it is also necessary to examine the viscosity for the prepared slurries of the tested groups. Fig. 6 b below shows the extracted viscosity data from the rheology testing for both 70 wt% and 80 wt%. From the above results, the impact of the solid loading was analysed. As can be seen in Fig. 6 b, when the solid loading concentration decreased from 75 wt% to 70 wt%, the slurry's viscosity fell significantly, reaching values considered unstable for printing due to the poor solid cohesion of the slurry itself, which tend to be more similar to a liquid than a viscous paste. As expected, when the solid loading decreases, the amount of the remaining resin and dispersant caused the slurry viscosity to fall. When the 70 wt% solid loading composition loaded into the reservoir of the printer and proceeded into the printing foil, it escaped from the printing region and accordingly failed to maintain its position in the building zone of the transported foil, resulting in the slurry being unusable to print solid parts (Fig. 6 c). On the other hand, when the solid loading was raised to 80 wt%, viscosity increased within acceptable values. This was then confirmed during the successful attempts to print the tested samples.

However, if the solid loading concentration is excessively high, the slurry's stability is compromised [42]. At lower shear rates, the slurry produced by the 75 wt% was relatively less viscous than the slurry produced by the 80 wt%. The high solid loading in the slurry could have a number of advantages, as it has been clearly reported in the literature that, by increasing the solid loading, the density of the printed part increased, promoting better mechanical strength and decreasing the shrinkage during sintering, hence lowering the insurgence of micro cracks [43]. Although the 75 wt% could still be considered acceptable, however, increasing the solid loading to higher values would make the connection between particle more stable at both green and brown stages [44]. Since the current study considers adding the dicalcium silicate where the material behaviour could not be anticipated, both slurries with 75 wt% and 80 wt% in solid loading were chosen for further examination.

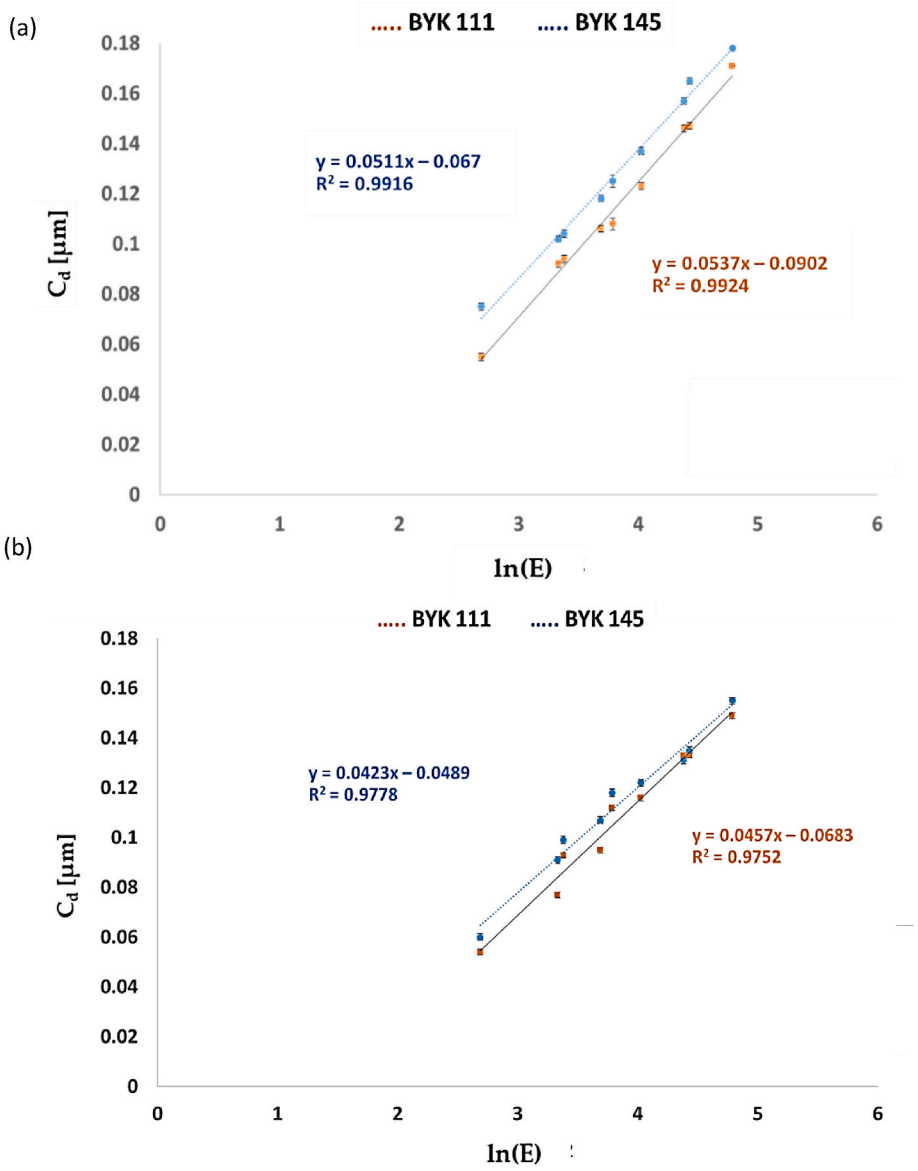

Fig. 3. (a) Cure depth for ADMATEC resin (b) Cure depth for ACMO/PEGDA/TPO resin.

3.4. DLP printing

A full DoE was implemented on both 75 wt% and 80 wt% solid loading groups to optimise the DLP printing parameters. This was designed to assess how variations in exposure energy, specifically, 200 %, 300 %, and 400 %, affect the curing depth, which is critical for achieving precise and consistent geometries. Additionally, the experiment investigated the effects of three different layer thicknesses, 20 µm, 25 µm, and 30 µm, on the curing performance, along with different exposure times for each test scenario. The calcium silicate was then added in three different ratios for each group, specifically, in 10 wt%, 30 wt% and 50 wt% contents. The results from each combination of parameters were evaluated to identify configurations that offered the best rheological characteristics and optimal curing depth.

The following figures illustrate the impact of the different parameters on the curing behaviour of the slurries. In Fig. 7a, the cure depth (Cd) for the 75 wt% solid loading slurry is plotted against the power (E) for different ratios of added calcium silicate. Similarly, Fig. 7b presents the same for the 80 wt% solid loading slurry. The data points across both figures fit well with the linear regression trend lines, indicating a predictable and consistent relationship between exposure power and cure depth. For the 75 wt% slurry (Fig. 7a), adding calcium silicate at different ratios (10 wt%, 30 wt%, and 50 wt%) slightly reduces the cure depth as the calcium silicate content increases. This suggests that higher calcium silicate concentrations might obstruct the penetration of light during curing, resulting in shallower depths. Conversely, for the 80 wt% slurry (Fig. 7b), the same trend is observed but with a more pronounced reduction in cure depth, particularly at the 50 wt% calcium silicate ratio. The higher solid loading exacerbates the reduction in cure depth, likely due to increased light scattering and reduced photopolymerization efficiency caused by the denser ceramic particle distribution. While Fig. 7 demonstrates that the 75 wt% solid loading slurry generally achieves better cure depth compared to the 80 wt% slurry. The 80 wt% slurry, despite exhibiting shallower cure depths, still achieves acceptable curing depth, particularly at lower calcium silicate ratios (10 wt% and 30 wt%).

Fig. 8 presents the viscosity data for both the 75 wt% and 80 wt% slurries, each with the addition of 10 wt% calcium silicate. Understanding the rheological behaviour of these slurries is crucial for determining their suitability for use with the Admaflex 130 DLP printer. Following the cure depth testing, a rheology assessment was conducted to evaluate the performance of each slurry in terms of its viscosity and

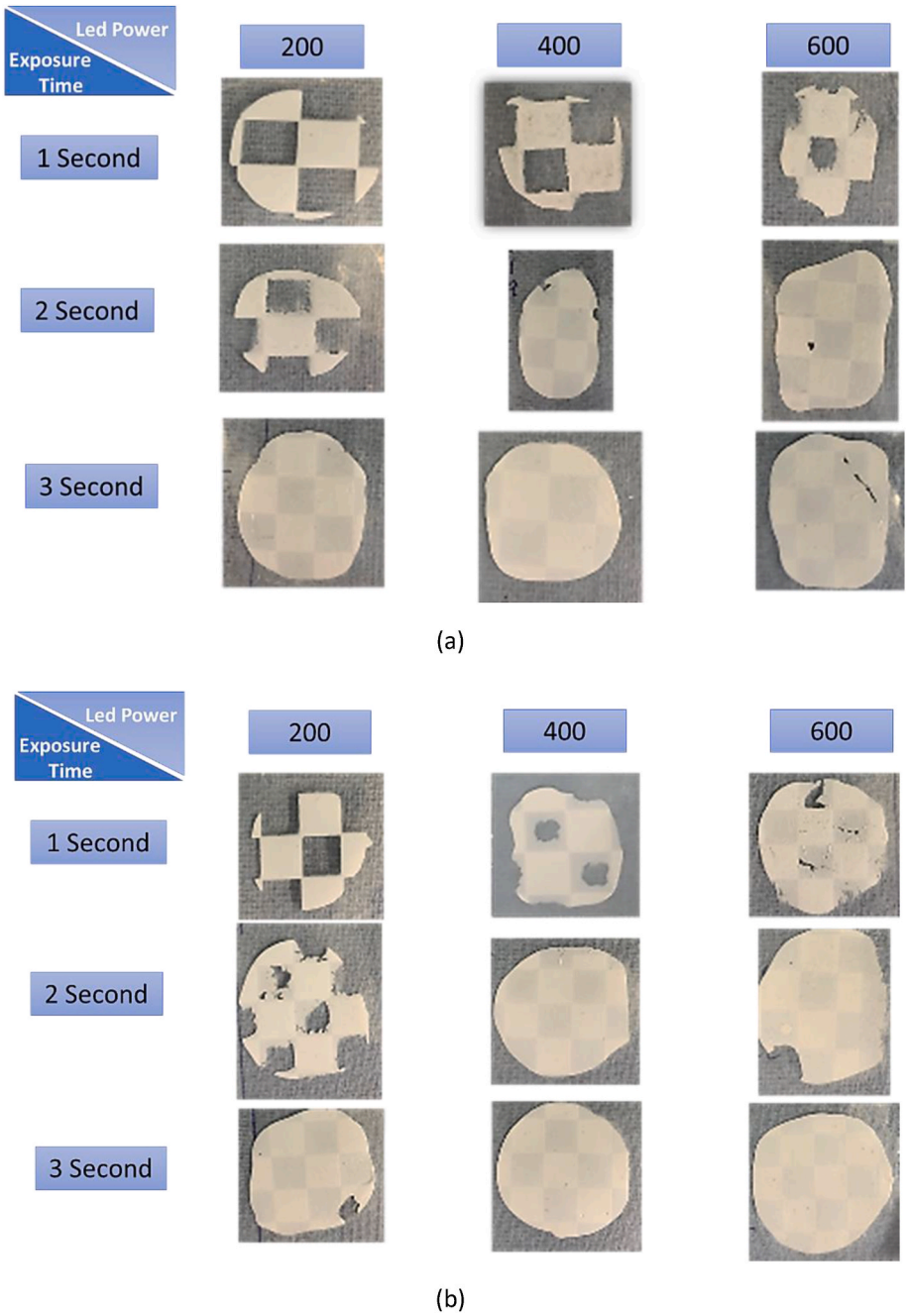

Fig. 4. (a) Checkboard shape printing accuracy using the ACMO/PEGDA resin with BYK-111 (b) Checkboard shape printing accuracy using the ACMO/PEGDA resin with BYK-145 dispersants.

flow properties. The group with the most favourable viscosity would be selected for printing, as this property significantly impacts the slurry's behaviour during the layer-by-layer deposition process in DLP.

The results from Fig. 8a reveal that the 80 wt% solid-loaded slurry exhibits a significantly higher viscosity than the 75 wt% slurry. This increased viscosity suggests that the higher solid loading enhances the mechanical properties by providing greater particle cohesion, but it also compromises printability due to the thicker, more resistant flow of the slurry. While this makes the 80 wt% slurry less ideal for smooth and uniform layer deposition, it also implies better stability during the curing and printing processes. In contrast, the 75 wt% slurry, with its lower viscosity, would flow more easily and provide smoother deposition, but it may lack the structural integrity needed for robust prints when subjected to the stresses of the DLP process. Fig. 8b further illustrates the impact of these viscosity differences on the actual printing process. During tape-casting, the 75 wt% slurry with 10 wt% calcium silicate failed to maintain cohesion, spilling out of the foil and demonstrating its inadequacy for stable layer formation. This result shows the limitations of using lower solid loading slurries as it fails to maintain sufficient structural integrity during DLP printing despite its smoother flow.

Previous studies highlight that adding calcium silicate can increase fluidity and reduce the viscosity level [45,46]. When 10 wt% calcium silicate was added to the 75 wt% slurry, its viscosity dropped below 0.5 Pa s. This reduction rendered the slurry unsuitable for use with the Admaflex 130 DLP printer, as it could no longer maintain a constant and uniform form during printing. This issue became apparent when attempting to print with the 75 wt% slurry, which spilled out of the

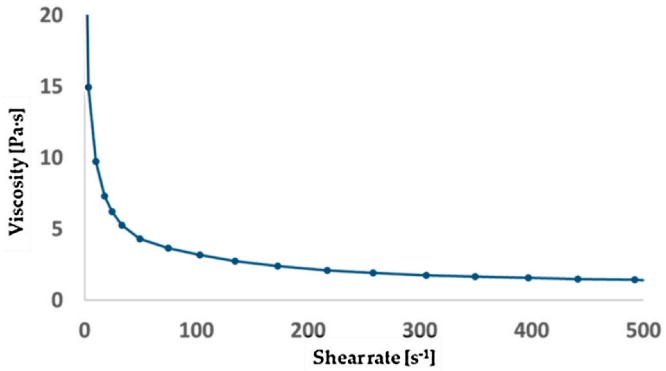

Fig. 5. Rheology testing BYK-111 and ACMO/PEGDA slurry.

tape-casting foil system, as shown in Fig. 8b. Given that the 75 wt% slurry with 10 wt% calcium silicate already exhibited inadequate viscosity, it was determined that further additions of calcium silicate at 30 wt% and 50 wt% would likely reduce the viscosity even more, making them impractical for use. Therefore, these compositions were excluded from further investigation. Conversely, all the 80 wt% solid-loaded slurries with the addition of 10 wt%, 30 wt%, and 50 wt% calcium silicate demonstrated favourable rheological properties and maintained cohesion during printing. While the increased viscosity of the 80 wt% slurry introduces potential challenges for precise and consistent deposition, especially in cases requiring intricate geometries, the stability and structural integrity of the 80 wt% slurries make them more suitable for high-performance DLP applications. As supported by the literature, higher solid loadings improve densification and lead to better printing outcomes. Therefore, the 80 wt% solid loading was selected for further investigation in this study, with the understanding that minor adjustments to printing parameters may be necessary to accommodate the thicker consistency without sacrificing print precision or detail.

In Fig. 9, the effect of varying layer thickness on the printing quality is examined across three different conditions: 20 µm, 25 µm, and 30 µm. The results indicate that thinner layers, such as 20 µm, face significant challenges, as many of the samples did not print successfully or fractured during removal, see Fig. 9a. Thinner layers require precise energy dosage and control to ensure proper curing, and any deficiency in this can lead to mechanical instability and weak bonding between the printed part and the substrate. This results in incomplete prints or difficulty in maintaining structural integrity during the process. Most likely, the difficulties in maintaining good adhesion in the case of small layer thickness were due to the small volume of the cured area. Curing an extremely thin layer would cause number of issues, such as delamination and gaps within the sample itself. On the other hand, smaller layer thicknesses, although known to improve the z-axis resolution, result in longer printing times, which makes it a less efficient option. Gibson et al. conducted an in-depth review of Additive Manufacturing technologies and addressed the difficulties linked to layer adhesion in 3D printing, specifically with thin layers [47].

Thinner layers, although able to enhance the resolution of the printed object, can result in challenges in maintaining adequate interlayer adhesion. This is due to a small volume of the cured material in each layer, which may not offer adequate bonding strength. Consequently, there is an increased risk of separation between layers. Furthermore, on some occasions, it was difficult to remove the samples from the printing base, which caused cracks on the samples upon removal, as shown using a red arrow in Fig. 9b. At 25 µm, some samples printed more successfully, but challenges persisted. fewer are shown as fractured, and other prints were incomplete, indicating that although an increase in layer thickness improves stability, the prints still experience mechanical stresses. This could be due to insufficient bonding between layers or uneven curing, resulting in a failure to withstand the stresses during the printing process or removal. However, at 30 µm, the samples printed smoothly and were successfully removed, demonstrating that this layer thickness provides better overall stability and structural integrity. The improved printing performance at this thickness can be attributed to more robust bonding between successive layers and greater mechanical strength, ensuring easier removal and higher-quality prints, Fig. 9c.

In Fig. 10, the effect of LED power and exposure time on the dimensional accuracy and curing behaviour of the 80 wt% solid loading slurry is examined. While some samples printed with a 30 µm layer thickness were successful, others showed significant deviations from their original CAD designs, particularly at higher exposure times and power settings. This deviation is largely attributed to the light scattering that occurs when excessive exposure power and time are applied. When the exposure time and power are too high, the same layer is exposed multiple times, leading to an increased cure depth and over-curing. As a result, sections of the printed objects deviate from their intended geometries, producing shapes that are significantly distorted compared to the original CAD models [48]. This overexposure phenomenon causes inaccuracies, especially in finer details, as the excessive energy causes the material to cure beyond the intended boundaries of each layer. The geometrical inaccuracies are primarily the result of the material being exposed to light for longer periods or at higher intensities than necessary, leading to poor control over the final dimensions of the printed object. Among the samples printed with 80 wt% solid loading and 30 µm layer thickness, those produced at exposure powers of 200 % demonstrated the highest dimensional accuracy. These settings helped avoid overexposure and ensured that each layer cured with the correct depth and precision, resulting in parts that closely matched the CAD designs. Additionally, the samples cured for 0.5 s and 0.750 s exhibited superior accuracy compared to those cured for longer periods, indicating that moderate exposure times are more effective in achieving accurate prints. Conversely, higher exposure powers and times, while potentially improving the strength of the cured layers, negatively impacted the accuracy of the prints. Lower exposure power and shorter curing times proved more effective in maintaining the integrity of the design, especially for fine geometrical details. Based on the reported results, the optimal printing parameters would be 0.75 s as exposure time, 300 ‰ as power dose, and 30 µm layer thickness. These factors showed the best quality and integrity in terms of accuracy and printability. Thus, these printing parameters were selected to produce the green parts that would subsequently undergo the debinding and sintering processes.

3.5. *Thermal post-processing*

3.5.1. *Debinding*

The decomposition of the printed green body during the debinding process is considered to be one of the most important steps when it comes to obtaining homogeneous samples without defects. The organic materials degradation during debinding were observed using the TGA-DSC curve, as presented in Fig. 11. This figure shows the thermal debinding process with the green curve indicates the percentage of the sample's remaining mass, which starts at 100 % and gradually decreases as temperature rises. Initially, a small mass loss of 5.13 % occurs between 34 °C and 366.2 °C, likely due to moisture and light volatiles. A significant mass loss of follows between 366.2 °C and 481.9 °C, corresponding to the breakdown of the primary binder. Subsequent smaller losses, from 481.9 °C to 616.1 °C, represent the decomposition of residual organics. By the end of the process, 76.37 % of the sample mass remains, representing the ceramic material after complete binder removal. The red curve (DTG) shows the rate of mass loss, peaking at 390.8 °C with the fastest binder degradation. As the temperature continues to rise, the rate of mass loss slows, with smaller peaks corresponding to additional phases of decomposition. The dashed red line represents the temperature ramp, reflecting steady heating that enables controlled binder removal without damaging the ceramic structure.

All samples were printed according to the determined printing

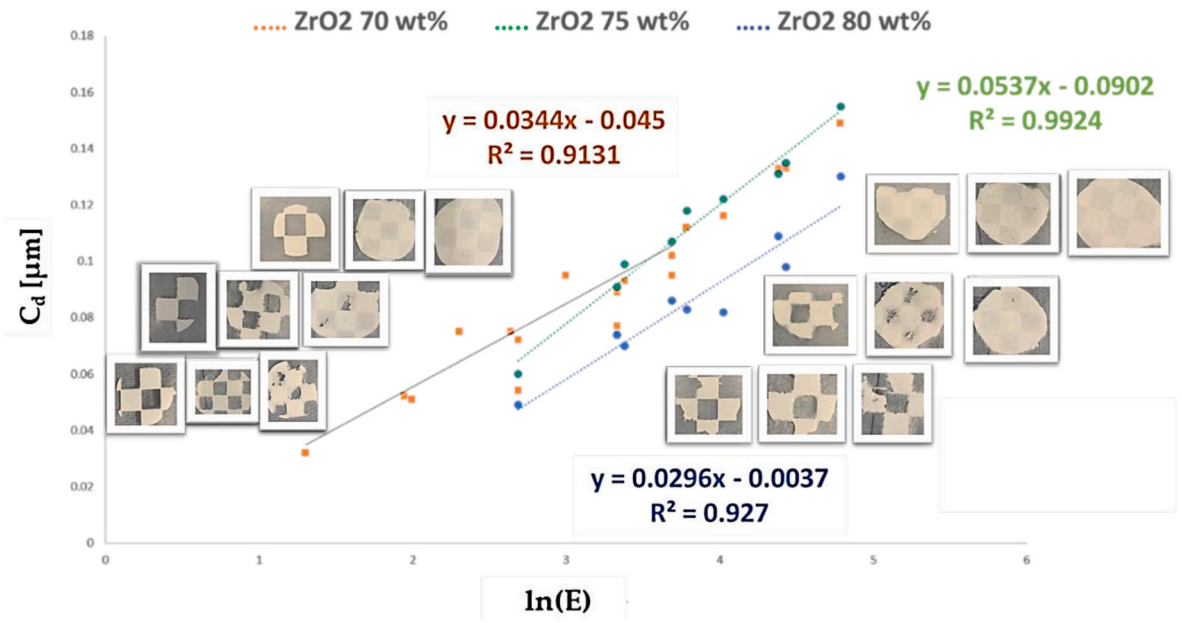

(a)

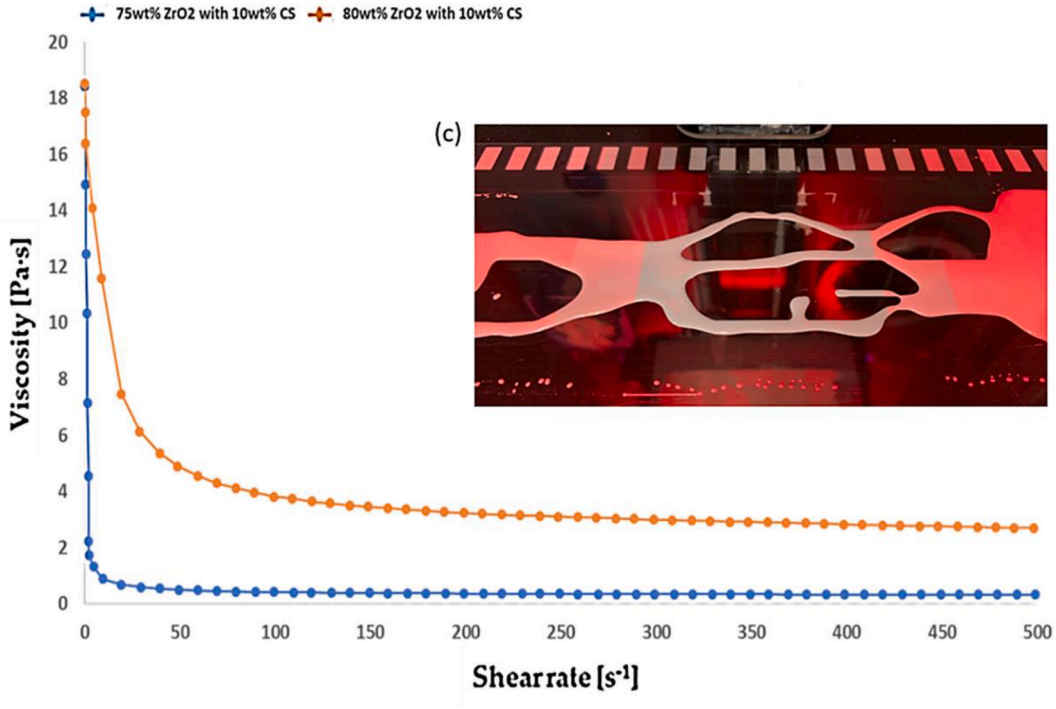

(b)

Fig. 6. (a) Cure depth and dimensional accuracy images (b) Rheology behaviour, (c) the fluidity of the 70 wt% solid loading slurry during DLP printing.

parameters and subjected to the appropriate debinding cycle. After being brought up from room temperature, the temperature was kept at 150 °C for 3 h to ensure initial solvent dehydration. After that, the temperature was raised to 380 °C and held for a dwell time of 3 h to allow the slow decomposition of the printed samples organic materials. This process, carried out slowly, facilitates the safe relief of the thermal stresses on the ceramic components. The temperature was then increased once again to reach 490 °C and maintained for another 3 h. To eliminate any remaining organic residue and pre-sinter the sample, the temperature was then raised gradually to 600 °C. The heating rate was controlled in accordance with the planned trial during the entire debinding, was kept at 0.2 °C/min.

It was reported that higher brown densities can be achieved using lower heating rates and longer dwell durations, which facilitate the progress of eliminating the binders over an extended period [49]. This process would effectively reduce the number of pores and accordingly

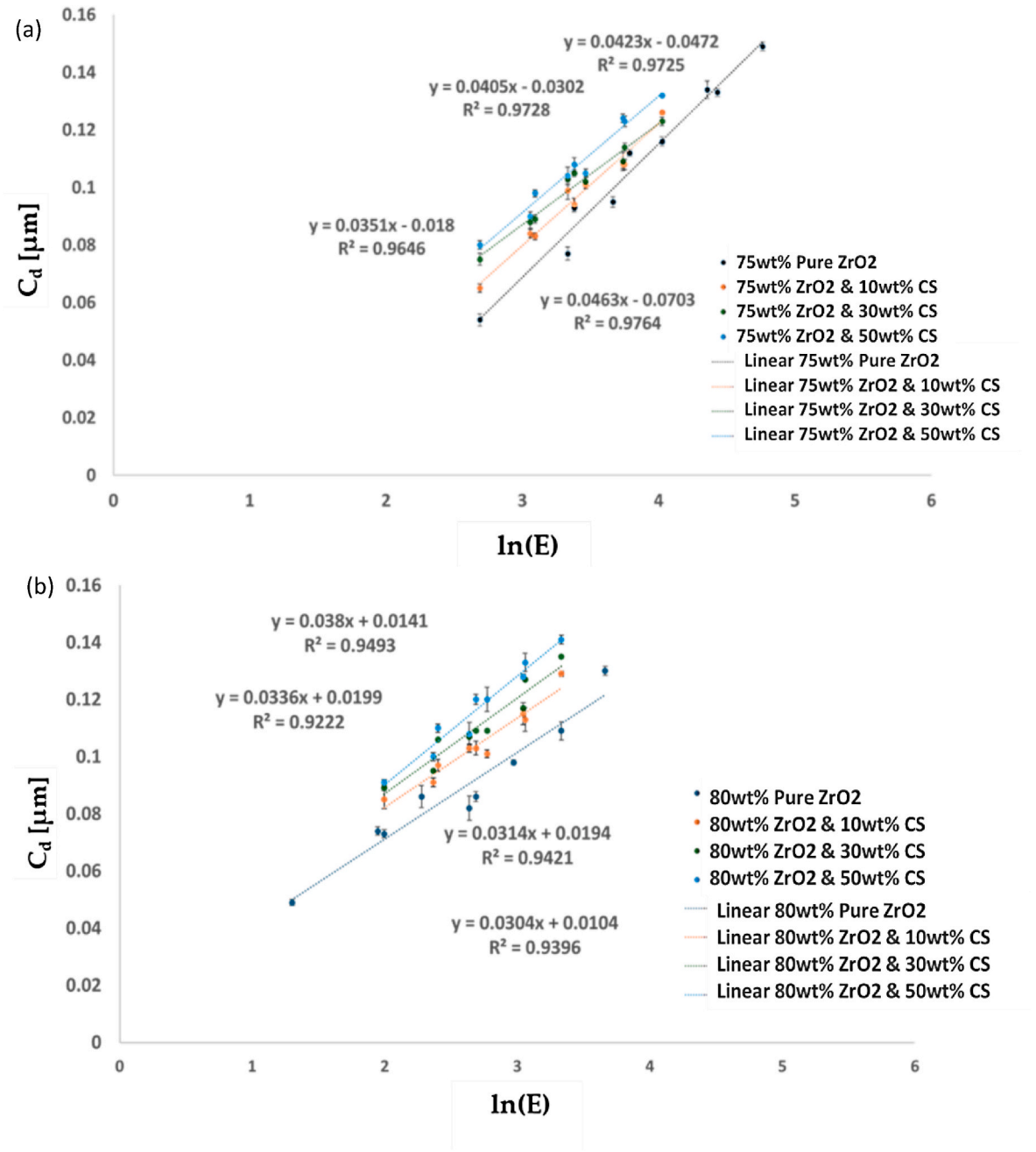

Fig. 7. (a) Cure depth of 75 wt% solid loading, along with the added calcium silicate in different ratios (b) Cure depth of 80 wt% solid loading, along with the added calcium silicate in different ratios.

improve the printed object density. This method additionally decreases thermal stresses, thereby decreasing the probability of sample cracking [50]. Moreover, gradual increases in temperature throughout transitions allow sufficient time for organic substances to depart from the ceramic structure, reducing the likelihood of defects and occurrence of cracks. Longer holding time at adequate high temperatures ensure the complete elimination of all organic materials from the sample.

3.5.2. Sintering

After completing the debinding cycle, the sintering cycle was investigated at 1300 °C and 1500 °C, see Fig. 12a. The DLP printed zirconia-Ca_2SiO_4 composite samples were divided into two groups and sintered in an air-sintering furnace with a heating rate of 3 °C/min and a dwell time of 3 h to enhance densification. However, during the sintering process, extended dwell times at high temperatures can lead to excessive grain growth, which negatively impacts the mechanical properties of the final dental units. SEM analysis of the samples sintered at 1300 °C shows a finer, more uniform grain structure with minimal porosity in the pure ZrO_2 sample, while increasing Ca_2SiO_4 content (10 %, 30 %, 50 %) progressively introduces more porosity and irregular grain boundaries, with the 50 % ZCS sample showing significant porosity and poor densification. At 1500 °C, the pure ZrO_2 and 10 % ZCS samples display significant grain growth and lower porosity, but larger grain sizes, particularly in the 30 % and 50 % ZCS samples, indicate excessive liquid-phase formation and poor consolidation. This grain coarsening at 1500 °C suggests a deterioration of mechanical properties, which is why the samples sintered at 1500 °C were excluded. Therefore, while the 1300 °C sintering process results in finer grains and better structural integrity for lower Ca_2SiO_4 content, higher temperatures (1500 °C) lead to oversized grains, which could undermine the

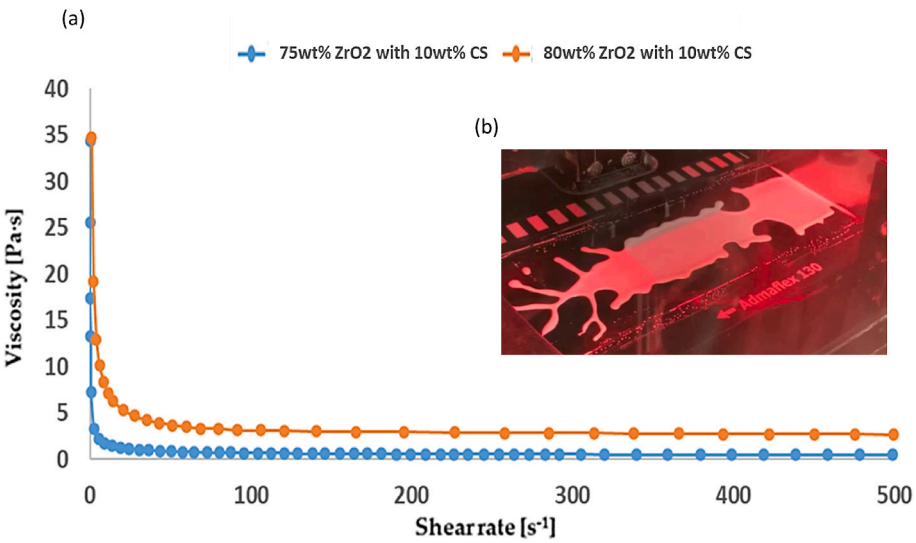

Fig. 8. (a) Viscosity data of the 75 wt% and 80 wt% solid loaded slurries with 10 wt% Ca2SiO4 (b) Cure depth of 80 wt% solid loading, along with the added calcium silicate in different ratios, (b) The 75 wt% with 10 wt% Ca2SiO4 failed and spilled out of tape-casting foil.

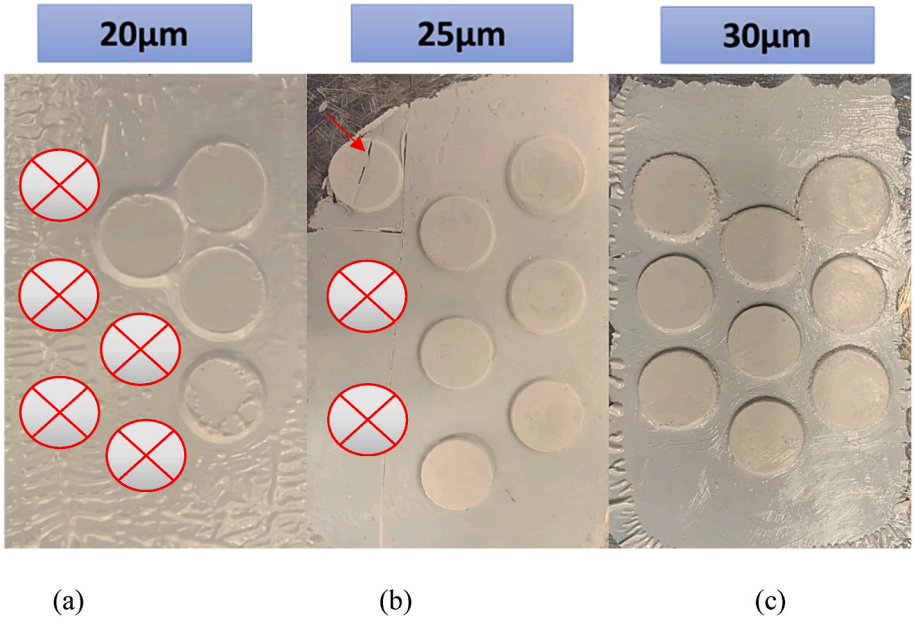

Fig. 9. Layer thicknesses effect on the printing quality: (a) Several samples did not print at 20 µm; (b) incomplete printing and fractured disc marked by an arrow in relation to existing difficulties during sample removal at 25 µm; (c) all samples successfully printed with no fracture occurrence at 30 µm.

mechanical performance of the composites.

To balance mechanical strength and bioactivity mechanical strength and bioactivity, it would be more optimal choice to sinter at a temperature of 1300 °C. This temperature allows for maintaining of the bioactive features of calcium silicate, whilst also ensuring sufficient densification and phase stability of zirconia. The findings of this study indicate that the samples sintered at 1300 °C were selected for their optimum mechanical properties. These samples demonstrated a relative density above 95 %, while those containing calcium silicate showed slightly lower relative densities, as seen in see Fig. 12b. However, the mechanical properties are expected to increase in line with an increase in the calcium silicate content, as their particles will aggregate and connect together, thus forming a form a cohesive network and enhance the overall mechanical performance of the material.

3.5.3. *Mechanical testing*

The compressive strength testing was conducted on the zirconia-calcium silicate composition that contains 30 % calcium silicate to assess the mechanical performance. The compression test value was 104.34 MPa, and the mechanical properties of the tested samples were obtained accordingly, as shown in Table 5 below. The results indicate the composition's capability to resist mastication forces and its ability to withstand applied loads in comparison to the mechanical abilities required for dental implants. The 30 % zirconia-calcium silicate composition was chosen for detailed analysis as it could provide a balance between the mechanical strength and biological activity factors, which are crucial for successful implant application. The achieved compressive strength underscores the material's durability for potential clinical use.

Dental implants required a balance between mechanical and biological properties. The obtained composite yield strength of 95.69 MPa

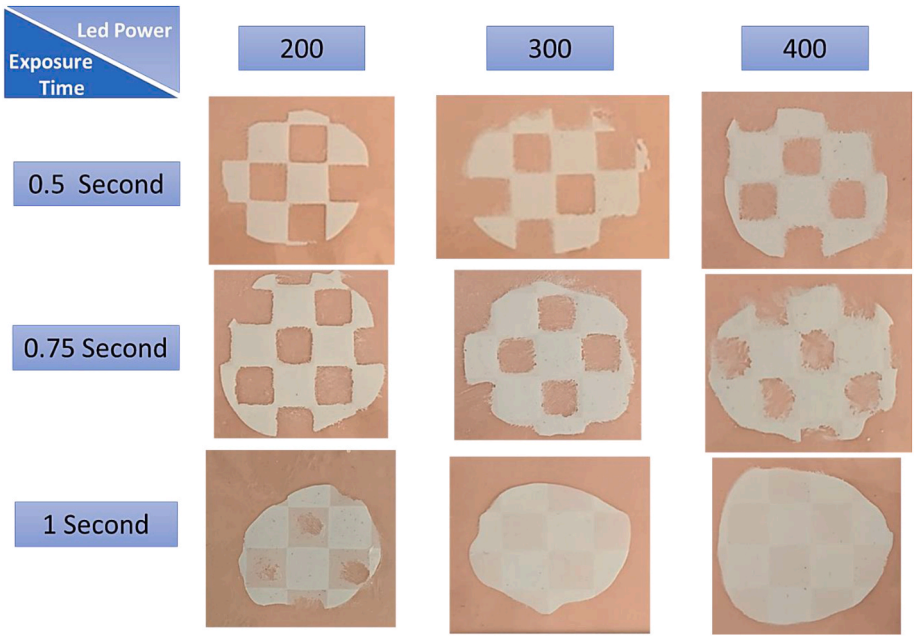

Fig. 10. Checkboard shape samples of the 80 wt% solid loading and layer thickness of 30 μm cured at different led power and exposure time.

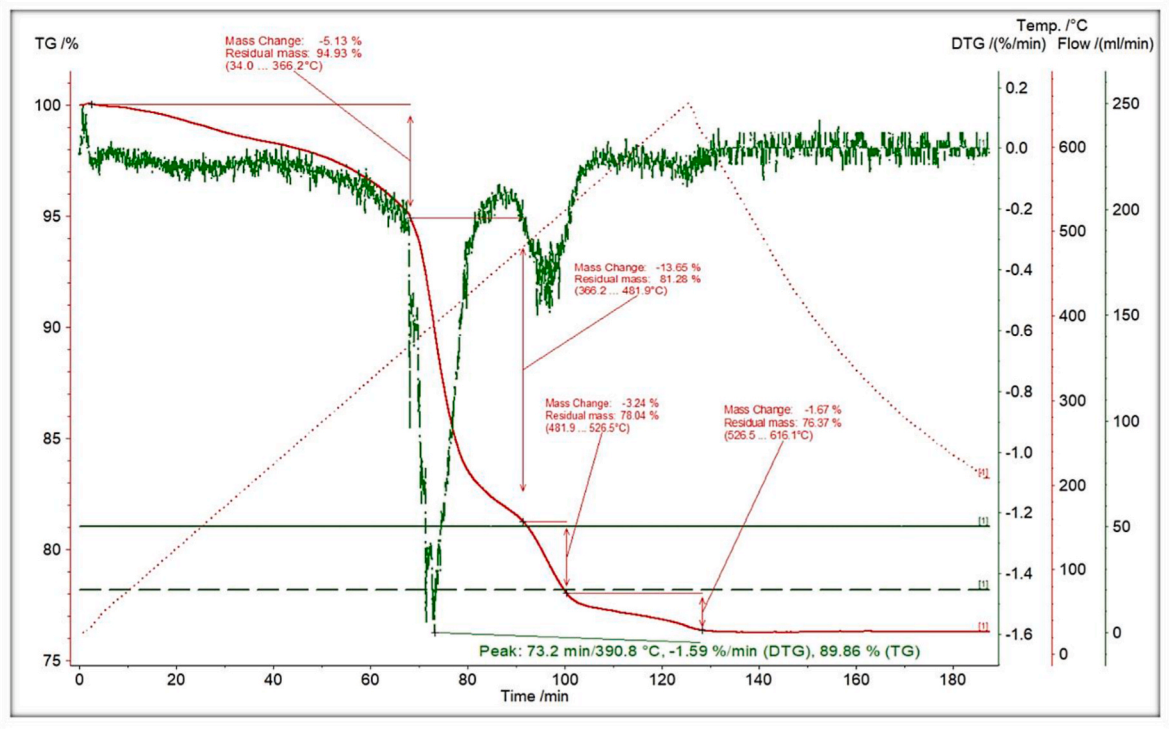

Fig. 11. Thermogravimetric Analysis of the ZrO2\CS sample.

and Young's modulus of 8.42 GPa are considered close values in comparison to the cancellous bone mechanical properties. This provides a chance for bone-like behaviour in implant applications. The presented results bear resemblance to some metal-polymer composites fabricated to mimic bone properties within the Young's modulus range of 4.4–24 GPs, potentially mitigating stress shielding and improving force distribution on the bone [51]. Various research concentrated on improving biological and mechanical properties as well as reducing the manufacturing cost while keeping the Young's modulus at the lowest possible to avoid stress shielding [52]. The yield strength is also consistent with the cancellous bone as maximum strength of cancellous bone was reported to be 8.78 ± 5.2 MPs [53].

4. Conclusions

This study introduced a novel bioactive material made from zirconia-calcium silicate ceramic slurries and optimized DLP printing with a focus on slurry composition, solid loading, calcium silicate, and DLP printing conditions to achieve a high print quality. BYK-111 was found to be an effective dispersant. Whereas using a resin composition of

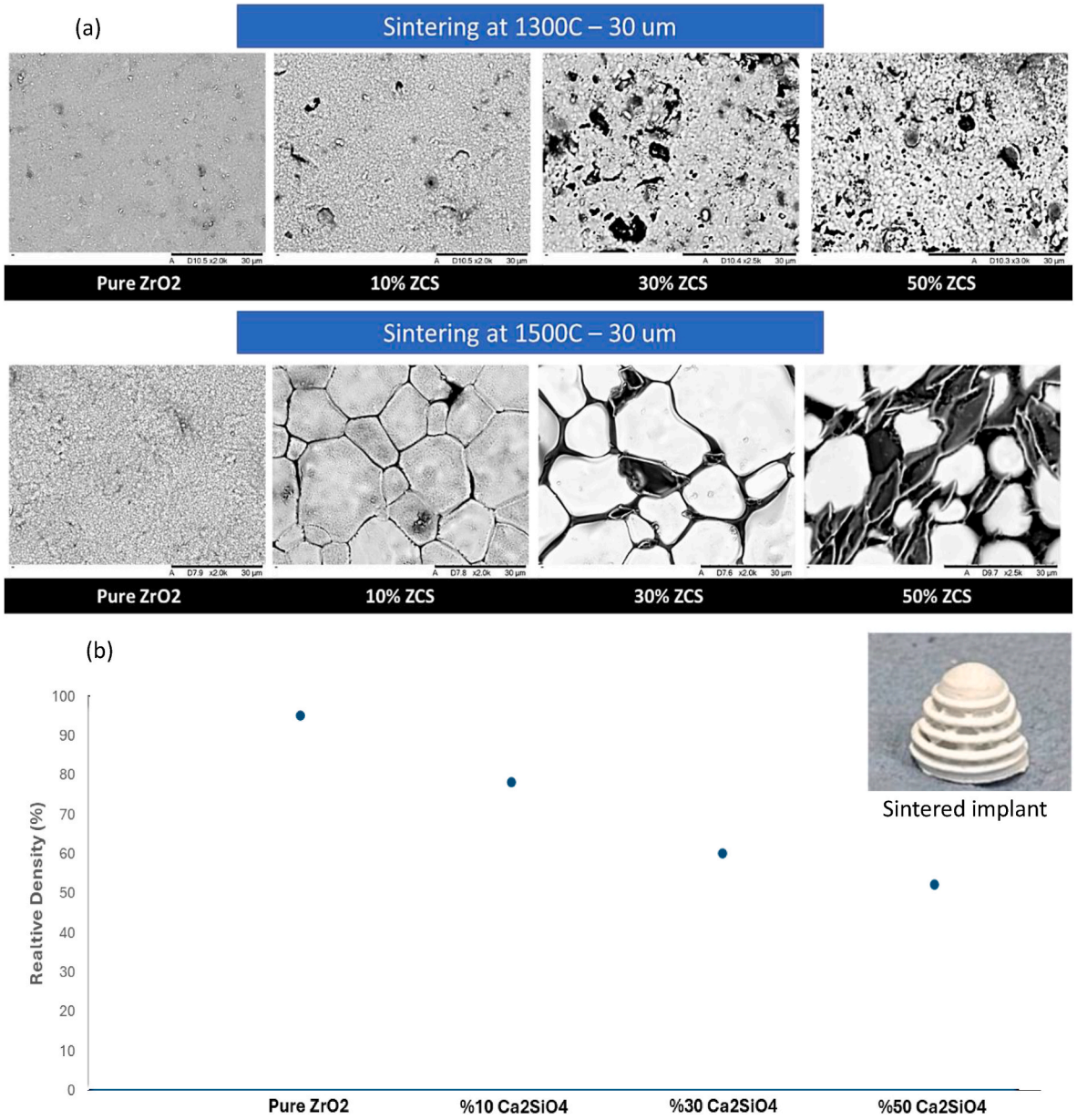

Fig. 12. (a) SEM images of sintered samples at different sintering temperatures for both different ZrO2\CS ratios (b) Relative density of the samples sintered at 1300 °C.

Table 5
Mechanical properties for the 30 % zirconia-calcium silicate composite.

Compressive strength (MPa)	Density (gr/cm3)	Yield Strength (MPa)	Young Modulus (GPa)
104.34	3.44	95.6	98.42

ACMO/PEGDA/TPO achieved the most suitable properties for DLP. On the other hand, the 80 wt% solid loading slurry was selected due to its favourable rheological and curing characteristics. A full factorial DoE revealed that exposure duration and power significantly influence the cure depth and overall print quality. The ideal DLP printing parameters were found to be an exposure time of 750 ms, exposure power of 300 %, and a layer thickness of 30 µm. Subsequent optimization of the debinding and sintering processes demonstrated that sintering at 1300 °C produced favourable microstructure samples compared to those sintered at 1500 °C, with SEM analysis showing that excessive grain growth at higher temperatures could compromise mechanical properties. The sintered samples were found to have a relative density exceeding 95 % for pure zirconia samples when sintered at 1300 °C. These results contribute to the field of introducing novel 3D printed biocoactive ceramic material, particularly for dental applications. This study demonstrates the zirconia-calcium silicate composite printability and material's capacity to withstand mechanical loads comparable to those encountered in dental and medical applications. Future research will focus on biological characterisation, and mechanical property evaluation to further validate the performance of the printed zirconia-calcium silicate ceramic materials.

CRediT authorship contribution statement

Ahmed Binobaid: Writing – original draft, Visualization, Validation, Software, Methodology, Investigation, Formal analysis. **Michele De Lisi:** Writing – original draft, Visualization, Validation, Software, Methodology, Investigation. **Josette Camilleri:** Writing – review &

editing, Validation, Supervision, Resources, Project administration, Investigation, Funding acquisition, Formal analysis, Conceptualization. **Hany Hassanin:** Writing – review & editing, Validation, Supervision, Investigation, Formal analysis, Data curation, Conceptualization. **Khamis Essa:** Writing – review & editing, Validation, Supervision, Resources, Project administration, Investigation, Funding acquisition, Formal analysis, Conceptualization.

Declaration of competing interest

The authors declare that they have no known competing financial interests or personal relationships that could have appeared to influence the work reported in this paper.

Data availability

Data will be made available on request.

References

[1] V.D.C. Nascimento, A.C.F. Conti, M.A. Cardoso, D.P. Valarelli, R.R. Almeida-Pedrin, Impact of orthodontic treatment on self-esteem and quality of life of adult patients requiring oral rehabilitation, Angle Orthod. 86 (5) (2016) 839–845, https://doi.org/10.2319/072215-496.1.

[2] M.A.V. Fadel, B.Z. Santos, R.P. Antoniazzi, L. Koerich, V.L. Bosco, A. Locks, Prevalence of malocclusion in public school students in the mixed dentition phase and its association with early loss of deciduous teeth, Dent. Press J. Orthod. 27 (4) (2022) e2220120, https://doi.org/10.1590/2177-6709.27.4.e2220120.oar.

[3] P. Wijk, J. Bouma, M.A.J. Waas, R. Oort, F.F.H. Rutten, The cost of dental implants as compared to that of conventional strategies, Int. J. Oral Maxillofac. Implants 13 (1998) 546–553.

[4] N. Dawod, M. Miculescu, I.V. Antoniac, F. Miculescu, D. Agop-Forna, Metal-ceramic Compatibility in dental restorations according to the metallic component manufacturing procedure, Materials 16 (16) (2023) 5556, https://doi.org/10.3390/ma16165556.

[5] L. Nistor, M. Grădinaru, R. Rîcă, P. Mărășescu, M. Stan, H. Manolea, A. Ionescu, I. Moraru, Zirconia use in dentistry - manufacturing and properties, Curr. Health Sci. J. 45 (1) (2019) 28–35, https://doi.org/10.12865/CHSJ.45.01.03.

[6] O. Santoliquido, P. Colombo, A. Ortona, Additive Manufacturing of ceramic components by Digital Light Processing: a comparison between the 'bottom-up' and the 'top-down' approaches, J. Eur. Ceram. Soc. (2019), https://doi.org/10.1016/j.jeurceramsoc.2019.01.044.

[7] Siddique, T.; Sami, I.; Nisar, M.; Naeem, M.; Karim, A.; Usman, M. Low Cost 3D Printing for Rapid Prototyping and its Application. 1–5. DOI: 10.1109/INTELLECT47034.2019.8954983.

[8] M. Dadkhah, J.-M. Tulliani, A. Saboori, L. Iuliano, Additive manufacturing of ceramics: advances, challenges, and outlook, J. Eur. Ceram. Soc. (2023), https://doi.org/10.1016/j.jeurceramsoc.2023.07.033.

[9] A. Bhatia, A.K. Sehgal, Additive manufacturing materials, methods and applications: a review, Mater. Today: Proc. 81 (2021), https://doi.org/10.1016/j.matpr.2021.04.379.

[10] F. Krujatz, A. Lode, J. Seidel, T. Bley, M. Gelinsky, J. Steingroewer, Additive Biotech-Chances, challenges, and recent applications of Additive Manufacturing technologies in biotechnology, N. Biotechnol. 39 (Pt B) (2017) 222–231, https://doi.org/10.1016/j.nbt.2017.09.001.

[11] J. Deckers, J. Vleugels, J. Kruth, Additive manufacturing of ceramics: a review, J. Ceram. Sci. Technol. 5 (2014) 245–260, https://doi.org/10.4416/JCST2014-00032.

[12] A. Villa, P. Gianchandani, F. Baino, Sustainable approaches for the additive manufacturing of ceramic materials, Ceramics 7 (2024) 291–309, https://doi.org/10.3390/ceramics7010019.

[13] N. Panhalkar, R. Paul, S. Anand, Increasing Part Accuracy in additive manufacturing processes using a k-d tree based clustered adaptive layering, J. Manuf. Sci. Eng. 136 (2014) 061017, https://doi.org/10.1115/1.4028586.

[14] S. Zakeri, M. Vippola, E. Levänen, A comprehensive review of the photopolymerization of ceramic resins used in stereolithography, Addit. Manuf. 35 (2020) 101177, https://doi.org/10.1016/j.addma.2020.101177.

[15] J.C. Wang, H. Dommati, Fabrication of zirconia ceramic parts by using solvent based slurry stereolithography and sintering, Int. J. Adv. Manuf. Technol. 98 (2018) 1537–1546, https://doi.org/10.1007/s00170-018-2349-3.

[16] B. Khoda, Computer-Aided Design of Additive Manufacturing Components, 2017, https://doi.org/10.1201/9781315151441-2.

[17] Y. Lakhdar, C. Tuck, J. Binner, A. Terry, R. Goodridge, Additive manufacturing of advanced ceramic materials, Prog. Mater. Sci. 116 (2021) 100736, https://doi.org/10.1016/j.pmatsci.2020.100736.

[18] G. Mitteramskogler, R. Gmeiner, R. Felzmann, S. Gruber, C. Hofstetter, J. Stampfl, J. Ebert, W. Wachter, J. Laubersheimer, Light curing strategies for lithography-based Additive Manufacturing of customized ceramics, Addit. Manuf. 1 (2014) 110–118, https://doi.org/10.1016/j.addma.2014.08.003.

[19] D.A. Komissarenko, P.S. Sokolov, A.D. Evstigneeva, I.A. Shmeleva, A.E. Dosovitsky, Rheological and curing behavior of acrylate-based suspensions for the DLP 3D printing of complex zirconia parts, Materials 11 (2018) 2350, https://doi.org/10.3390/ma11122350.

[20] M. Griffith, J. Halloran, Ultraviolet Curable Ceramic Suspensions for Stereolithography of Ceramics, vol. 68, American Society of Mechanical Engineers, Production Engineering Division (Publication) PED, 1994, pp. 529–534.

[21] G. Tarı, J.M.F. Ferreira, Influence of solid loading on drying-Shrinkage behaviour of slip cast bodies, J. Eur. Ceram. Soc. 18 (5) (1998) 487–493, https://doi.org/10.1016/S0955-2219(97)00161-1.

[22] D.A. Komissarenko, P.S. Sokolov, A.D. Evstigneeva, I.A. Shmeleva, A.E. Dosovitsky, Rheological and curing behavior of acrylate-based suspensions for the DLP 3D printing of complex zirconia parts, Materials 11 (2018) 2350, https://doi.org/10.3390/ma11122350.

[23] K. Zhang, C. Xie, G. Wang, R. He, G. Ding, M. Wang, D. Dai, D. Fang, High solid loading, low viscosity photosensitive Al2O3 slurry for stereolithography based additive manufacturing, Ceram. Int. 45 (2019) 203–208, https://doi.org/10.1016/j.ceramint.2018.09.152.

[24] Y. Wu, J. Liu, L. Kang, J. Tian, X. Zhang, J. Hu, Y. Huang, F. Liu, H. Wang, Z. Wu, An overview of 3D printed metal implants in orthopedic applications: present and future perspectives, Heliyon 9 (7) (2023) e17718, https://doi.org/10.1016/j.heliyon.2023.e17718.

[25] H. Hassanin, K. Jiang, Fabrication and characterization of stabilised zirconia micro parts via slip casting and soft moulding, Scripta Mater. 69 (6) (2013) 433–436, https://doi.org/10.1016/j.scriptamat.2013.05.004.

[26] H. Hassanin, K. Jiang, Optimized process for the fabrication of zirconia micro parts, Microelectron. Eng. 87 (5–8) (2010) 1617–1619, https://doi.org/10.1016/j.mee.2009.10.037.

[27] H. Hassanin, K. Jiang, Net shape manufacturing of ceramic micro parts with tailored graded layers, J. Micromech. Microeng. 24 (1) (2013) 015018, https://doi.org/10.1088/0960-1317/24/1/015018.

[28] A. Ghayoor, A.S. Khan, N. Aslam, Calcium silicate: a smart scaffold for bone tissue engineering, SN Appl. Sci. 2 (1) (2020) 1–9, https://doi.org/10.1007/s43188-019-00013-1.

[29] H. Zhang, C. Jiao, Z. Liu, Z. He, M. Ge, Z. Tian, C. Wang, Z. Wei, L. Shen, H. Liang, 3D-Printed composite, calcium silicate ceramic doped with CaSO4·2H2O: degradation performance and biocompatibility, J. Mech. Behav. Biomed. Mater. 121 (2021) 104642, https://doi.org/10.1016/j.jmbbm.2021.104642.

[30] S. Yang, P. Wu, Calcium silicate improved bioactivity and mechanical properties of poly(3-hydroxybutyrate-co-3-hydroxyvalerate) scaffolds, Polymers 9 (2017) 175, https://doi.org/10.3390/polym9050175.

[31] F. Kermani, A.H. Rezayan, Three-dimensional printing of calcium silicate scaffolds, Iranian Journal of Science and Technology, Transactions A: Science 42 (1) (2018) 235–240, https://doi.org/10.1007/s13758-018-0183-y.

[32] S.J. Ding, Y.H. Chu, P.T. Chen, Mechanical biocompatibility, osteogenic activity, and antibacterial efficacy of calcium silicate-zirconia biocomposites, ACS Omega 6 (10) (2021) 7106–7118, https://doi.org/10.1021/acsomega.1c00097.

[33] G. Varghese, M. Moral, M. Castro-Garcia, J. López-López, J. Marín-Rueda, V. Yagüe-Alcaraz, L. Afonso, J.C. Ruiz-Morales, J. Canales-Vázquez, Fabrication and characterisation of ceramics via low-cost DLP 3D printing, Bol. Soc. Espanola Ceram. Vidr. 57 (2017), https://doi.org/10.1016/j.bsecv.2017.09.004.

[34] N.A. Nawafleh, F. Mack, J. Evans, J. Mackay, M.M. Hatamleh, Accuracy and reliability of methods to measure marginal adaptation of crowns and FDPs: a literature review, J. Prosthodont. 22 (5) (2013) 419–428, https://doi.org/10.1111/jopr.12006.

[35] D.A. Komissarenko, P.S. Sokolov, A.D. Evstigneeva, I.A. Shmeleva, A.E. Dosovitsky, Rheological and curing behavior of acrylate-based suspensions for the DLP 3D printing of complex zirconia parts, Materials 11 (2018) 2350, https://doi.org/10.3390/ma11122350.

[36] J. Bennett, Measuring UV curing parameters of commercial photopolymers used in additive manufacturing, Addit. Manuf. 18 (2017) 203–212, https://doi.org/10.1016/j.addma.2017.10.009.

[37] C.M. Cristache, S. Gurbanescu, Accuracy evaluation of a stereolithographic surgical template for dental implant insertion using 3D superimposition protocol, Int. J. Dent. 2017 (2017) 4292081, https://doi.org/10.1155/2017/4292081.

[38] G. Liu, C. Yan, K. Zhang, H. Jin, R. He, Effect of solid loading on the property of Al2O3 ceramics in stereolithographic additive manufacturing, J. Inorg. Mater. 37 (2021) 636, https://doi.org/10.15541/jim20210636.

[39] S.P. Kochar, A. Reche, P. Paul, The etiology and management of dental implant failure: a review, Cureus 14 (2022) e30455, https://doi.org/10.7759/cureus.30455.

[40] A.S. Jati, L.Z. Furquim, A. Consolaro, Gingival recession: its causes and types, and the importance of orthodontic treatment, Dent. Press J. Orthod. 21 (2016) 18–29, https://doi.org/10.1590/2177-6709.21.3.018-029.oin.

[41] B. Nugala, B.S. Kumar, S. Sahitya, P.M. Krishna, Biologic width and its importance in periodontal and restorative dentistry, J. Conserv. Dent. 15 (2012) 12–17, https://doi.org/10.4103/0972-0707.92599.

[42] K. Zhang, C. Xie, G. Wang, R. He, G. Ding, M. Wang, D. Dai, D. Fang, High solid loading, low viscosity photosensitive Al2O3 slurry for stereolithography based additive manufacturing, Ceram. Int. 45 (2019) 203–208, https://doi.org/10.1016/j.ceramint.2018.09.152.

[43] P. Cai, L. Guo, H. Wang, J. Li, J. Li, Y. Qiu, Q. Zhang, Q. Lue, Effects of slurry mixing methods and solid loading on 3D printed silica glass parts based on DLP stereolithography, Ceram. Int. 46 (2020), https://doi.org/10.1016/j.ceramint.2020.03.260.

[44] P. Tomasik, C.H. Schilling, R. Jankowiak, J.C. Kim, The role of organic dispersants in aqueous alumina suspensions, J. Eur. Ceram. Soc. 23 (2003) 913–919, https://doi.org/10.1016/s0955-2219(02)00204-2.
[45] D. Min, Effect of fluorspar and alumina on the viscous flow of calcium silicate melts containing MgO, J. Non-Cryst. Solids 337 (2004) 150–156, https://doi.org/10.1016/j.jnoncrysol.2004.03.109.
[46] K. Schumacher, J. White, J. Downey, Viscosities in the calcium–silicate slag system in the range of 1798 K to 1973 K (1525 °C to 1700 °C), Metall. Mater. Trans. B 46B (2015) 119–124, https://doi.org/10.1007/s11663-014-0173-1.
[47] I. Gibson, D. Rosen, B. Stucker, Additive Manufacturing Technologies: 3D Printing, Rapid Prototyping, and Direct Digital Manufacturing, second ed., Springer, New York, NY, 2015 https://doi.org/10.1007/978-1-4939-2113-3.
[48] L.N. Khanlar, A. Salazar Rios, A. Tahmaseb, A. Zandinejad, Additive manufacturing of zirconia ceramic and its application in clinical dentistry: a review, Dent. J. 9 (2021) 104, https://doi.org/10.3390/dj9090104.
[49] J.H. Sim, B.K. Koo, M. Jung, D.S. Kim, Study on debinding and sintering processes for ceramics fabricated using digital light processing (DLP) 3D printing, Processes 10 (2022) 2467, https://doi.org/10.3390/pr10112467.
[50] L. Zhang, J. Huang, Z. Xiao, Y. He, K. Liu, B. He, B. Xiang, J. Zhai, L.B. Kong, Effects of debinding condition on microstructure and densification of alumina ceramics shaped with photopolymerization-based additive manufacturing technology, Ceram. Int. 48 (2022), https://doi.org/10.1016/j.ceramint.2022.01.288.
[51] I.V. Okulov, J. Weissmüller, J. Markmann, Dealloying-based interpenetrating-phase nanocomposites matching the elastic behavior of human bone, Sci. Rep. 7 (1) (2017) 20, https://doi.org/10.1038/s41598-017-00048-4.
[52] M. Abdel-Hady Gepreel, M. Niinomi, Biocompatibility of Ti-alloys for long-term implantation, J. Mech. Behav. Biomed. Mater. 20 (2013) 407–415, https://doi.org/10.1016/j.jmbbm.2012.11.014.
[53] G. Poumarat, P. Squire, Comparison of mechanical properties of human, bovine bone and a New processed bone xenograft, Biomaterials 14 (5) (1993) 337–340, https://doi.org/10.1016/0142-9612(93)90051-3.